Journal of Power Sources 216 (2012) 281–289

Contents lists available at SciVerse ScienceDirect

Journal of Power Sources

journal homepage: www.elsevier.com/locate/jpowsour

Preparation, structural characterization and catalytic properties of Co/CeO_2 catalysts for the steam reforming of ethanol and hydrogen production

Adriana S.P. Lovón [a], Juan J. Lovón-Quintana [a], Gizelle I. Almerindo [a], Gustavo P. Valença [a], Maria I.B. Bernardi [b], Vinícius D. Araújo [b], Thenner S. Rodrigues [c], Patrícia A. Robles-Dutenhefner [c], Humberto V. Fajardo [c,*]

[a] Faculdade de Engenharia Química, Universidade Estadual de Campinas, UNICAMP, 13083-970, Campinas – SP, Brazil
[b] Instituto de Física de São Carlos, Universidade de São Paulo, USP, 13560-970, São Carlos – SP, Brazil
[c] Departamento de Química, Universidade Federal de Ouro Preto, Campus Universitário s/n Bauxita, UFOP, 35400-000, Ouro Preto – MG, Brazil

HIGHLIGHTS

- Ceria-supported cobalt catalysts, with different cobalt contents, were prepared by the polymeric precursor method.
- The catalysts were evaluated for the steam reforming of ethanol for hydrogen production.
- The cobalt content of the catalyst influences the metal-support interaction which results in distinct catalyst performances.
- The catalyst with the highest cobalt content showed the best performance among the catalysts tested.

ARTICLE INFO

Article history:
Received 2 February 2012
Received in revised form
22 May 2012
Accepted 23 May 2012
Available online 30 May 2012

Keywords:
Cobalt
Cerium
Ethanol steam reforming
Hydrogen
Pechini method

ABSTRACT

In this paper, Co/CeO_2 catalysts, with different cobalt contents were prepared by the polymeric precursor method and were evaluated for the steam reforming of ethanol. The catalysts were characterized by N_2 physisorption (BET method), X-ray diffraction (XRD), UV–visible diffuse reflectance, temperature programmed reduction analysis (TPR) and field emission scanning electron microscopy (FEG-SEM). It was observed that the catalytic behavior could be influenced by the experimental conditions and the nature of the catalyst employed. Physical–chemical characterizations revealed that the cobalt content of the catalyst influences the metal-support interaction which results in distinct catalyst performances. The catalyst with the highest cobalt content showed the best performance among the catalysts tested, exhibiting complete ethanol conversion, hydrogen selectivity close to 66% and good stability at a reaction temperature of 600 °C.

1. Introduction

As investment continues to grow in a clean fuel economy, hydrogen, one of the most abundant elements on earth, is an attractive alternative to traditional fuel sources as a sustainable energy for the near future. In combination with fuel cells, it has been proposed as a major energy source which could contribute to the reduction of atmospheric pollution and greenhouse gas emissions and reduction of global dependency on fossil fuels. Nowadays, the main process for hydrogen production is the steam reforming of natural gas, which is based on a fossil resource and is always associated with the emissions of local pollutants. Therefore, due to the expected increasing demand for energy together with environmental concerns related to reducing atmospheric pollution, the development of alternative methods for hydrogen production, especially from renewable sources, has been attracting much attention [1–5]. An alternative and promising way for producing hydrogen, that has attracted attention of researchers worldwide, is to use ethanol as a feedstock for the steam reforming process. Ethanol has several advantages when compared to fossil fuels but the most important is probably its renewable origin. Ethanol can be easily obtained from several biomass sources such as the fermentation of sugarcane (also called bioethanol) which is very interesting for Latin American countries with extensive plantations of this crop. In particular, Brazil has a very successful sugarcane industry and leads the world in the production and use of ethanol from sugarcane for fuel. The bioethanol-to-hydrogen system has

* Corresponding author. Tel.: +55 31 3559 1230; fax: +55 31 35591660.
E-mail address: hfajardo@iceb.ufop.br (H.V. Fajardo).

0378-7753
doi:10.1016/j.jpowsour.2012.05.066

the positive feature of being CO_2 neutral, thus environmental friendly, since the CO_2 produced is consumed for biomass growth and a nearly closed carbon cycle results. Moreover, ethanol has relatively high hydrogen content, and its reaction with water under steam reforming conditions has been shown to be theoretically feasible from a thermodynamic point of view [6–10]. Several publications report experimental catalytic studies for the above-mentioned reaction, discussing the utilization of different oxides and noble- and non-noble metal-based catalysts. From the data reported, catalytic performance appears to be influenced not only by the operational conditions employed, but also the nature of the metal phase and support used. Nobel metal-based catalysts frequently exhibit better activity when compared to non-noble metal catalysts, however, these catalysts are very expensive. As a less expensive alternative, cobalt-based catalysts have been shown to have high activity and selectivity toward hydrogen, due to their capacity for C–C bond cleavage. Generally, acidic supports, such as Al_2O_3, are known to favor the dehydration reactions to ethylene and diethyl ether, followed by polymerization of ethylene to form coke. Basic supports, such as MgO, favor dehydrogenation and condensation reactions producing acetaldehyde and acetone. The presence of these undesirable products, generated from these reactions, hinders the overall hydrogen production reducing the catalyst selectivity towards H_2 [11–14]. However, better catalytic performance with good stability and high hydrogen selectivity can be expected over supports with redox properties, such as CeO_2. This oxide has been commonly used as catalyst or catalyst support, as well as an effective promoter for catalysts, in the ethanol steam reforming process. This oxide has high oxygen mobility and storage capacity, and can act as a local source or sink for oxygen involved in reactions taking place on its surface. Notably, cerium oxide is known to enhance the reducibility, stability and the dispersion of the supported metal [15–28].

The objective of the present study was to prepare a bifunctional catalyst, based on cobalt and cerium for efficient steam reforming of ethanol to produce hydrogen with high selectivity. The catalysts were prepared through the polymeric precursor method. This method, also called the Pechini method, allows the production of nanocrystalline powder samples at relatively low temperatures. This synthesis produces a polymer network starting from a poly-hydroxy-alcohol and an alpha-hydroxycarboxylic acid, with metallic cations homogeneously distributed throughout the matrix [29]. The catalytic behavior in the ethanol steam reforming for hydrogen production was investigated by evaluating the effect of reaction temperature and cobalt content.

2. Experimental

2.1. Sample preparation

Ceria-supported cobalt catalysts were synthesized by the polymeric precursor method, following the procedure described in a previous report [30]. Briefly, cerium ammonium nitrate, $(NH_4)_2Ce(NO_3)_6$ – Aldrich, and cobalt nitrate, $Co(NO_3)_2 \cdot 6H_2O$ – Vetec, were used as precursors. The cerium ammonium nitrate and cobalt nitrate were dissolved in water and then mixed into an aqueous citric acid solution (100 °C) under constant stirring. The pH of the solution was adjusted to 6.0 with ammonium hydroxide solution. Next, ethylene glycol was added to polymerize the citrate by a polyesterification reaction. The citric acid:metal molar ratio was 3:1, while the citric acid:ethylene glycol mass ratio was 60:40. The resulting polymer resin was then calcined at 600 °C for 2 h to produce $(x)Co/CeO_2$ samples, where x (%mol) was equal to 5, 10, 15 and 20, respectively.

2.2. Sample characterization

The specific surface area (BET method) was measured by the N_2 adsorption/desorption isotherms at liquid nitrogen temperature, using a Micromeritics ASAP 2000. The equivalent spherical diameter of the particles, d_{BET}, was calculated with the equation: $d_{BET} = 6/S_s\rho$, where S_s is the specific surface area and ρ is the density of the material in the particles.

The powders were structurally characterized with an automatic X-ray diffractometer (Rigaku, Rotaflex RU200B) with CuKα radiation (50 kV, 100 mA, λ = 1.5405 Å) equipped with a graphite monochromator. The θ–2θ configuration was used, 2θ ranging between 20 and 90°, with a step size of 0.02° and a step time of 5.0 s. Rietveld analysis was performed with the Rietveld refinement program GSAS [31]. A pseudo-Voigt profile function was used.

UV–visible diffuse reflectance spectra were acquired with a Cary 5G spectrophotometer in the 200–800 nm range.

The morphology of the samples was investigated by field emission scanning electron microscopy using a (FEG-SEM, Zeiss Supra™ 35) equipment.

Temperature programmed reduction (TPR) analysis in a 5%H_2/N_2 (95 cm^3 min^{-1}) gas mixture were carried out in a ChemBET TPR/TPD Quantachrome instrument. The samples were previously treated *in situ* under a He atmosphere (95 cm^3 min^{-1}) at 200 °C for 2 h. The heat-treated samples were heated in the gas mixture from room temperature to 900 °C with a heating rate of 10°C min^{-1}.

2.3. Catalytic tests

Catalytic tests were carried out at atmospheric pressure in a fixed-bed quartz tubular reactor, 6 mm of inner diameter, packed with 10 mg of catalyst placed in an oven (EDG model 10P-S) at 400, 500 and 600 °C. Prior to reaction, the catalysts were heat-treated under hydrogen atmosphere at 450 °C for 1.5 h at a flow rate of 50 cm^3 min^{-1}. Water and ethanol were fed into the reactor using a system with two saturators to obtain a water:ethanol molar ratio of 3.1 ± 0.1. Helium was used as carrier gas at a total flow rate of 30 cm^3 min^{-1}. The reactants and the reaction products were analyzed by gas chromatograph (Agilent 7890A), equipped with a thermal conductivity detector (TCD) and a flame ionization detector (FID) connected in series. The chromatograph columns used were the HP-Plot-Q and an HP-Molesieve both with 30 m in length and 0.53 mm in diameter.

3. Results and discussion

3.1. Sample characterization

The specific surface area of the CeO_2 sample prepared in this work was 40.4 m^2 g^{-1} (Table 1). The specific surface area of all samples varied between 27.7 and 48.1 m^2 g^{-1}. However, the value of the specific surface area oscillates as the amount of Co increases from 0 to 20% of the metal atom content. No change in the value of

Table 1
Specific surface area (s_{bet}), lattice parameter (a), oxygen occupancy (O_{occup}), density (ρ) and equivalent spherical diameter (d_{eq}) of ceria-supported cobalt samples.

Sample	S_{BET} (m^2 g^{-1})	a (Å)[a]	O_{occup}[a]	ρ (g cm^{-3})[a]	d_{eq} (nm)
CeO_2	40.4	5.416(4)	0.97(0)	7.158	21
(5)Co/CeO_2	40.4	5.416(5)	0.94(2)	6.967	21
(10)Co/CeO_2	34.6	5.414(9)	0.95(6)	7.147	24
(15)Co/CeO_2	48.1	5.417(0)	0.97(2)	7.157	17
(20)Co/CeO_2	27.7	5.418(3)	0.93(1)	7.110	30

[a] calculated via refinement Rietveld.

the specific surface area was observed for the (5)Co/CeO_2 sample. In comparison, a decrease in the specific surface area was observed at 10% cobalt content ((10)Co/CeO_2) but then an increase for the (15) Co/CeO_2 sample and a subsequently decrease again for the (20)Co/ CeO_2 sample. The equivalent spherical diameter of the particles (d_{eq}) varied between 17 and 30 nm, all in the nanometric range.

Fig. 1 shows the XRD patterns of the ceria-supported cobalt samples. Fluorite type CeO_2 (ICSD n° 156250) was present in all the samples. Secondary phase peaks were found in the samples with 10, 15 and 20% of cobalt. Table 1 describes the lattice parameter (a) and oxygen occupancy calculated from the Rietveld refinement. The lattice parameter a does not vary monotonically with composition. First, there is a decrease in a up to 10% cobalt, followed by an increase in a for samples with 15 and 20% cobalt. A decrease in oxygen occupancy occurs with increasing cobalt content. This decrease in oxygen occupancy is related to an increase in the content of oxygen vacancies in the ceria matrix to preserve electron neutrality, as proposed elsewhere [32]. The decrease in the lattice parameter of ceria-supported cobalt samples has been associated with the substitution of bigger Ce^{4+} ion (radii = 0.97 Å) by the smaller Co^{2+} ion (radii = 0.90 Å) or Co^{3+} ion (radii = 0.61 Å) [33,34]. The increase in lattice constant is explained in terms of strains in the lattice generated by an increasing molar fraction of oxygen vacancies [35]. Hence, it is possible that these two effects coexist and contribute in altering the lattice parameter of the samples. Thus, it is believed that the decrease in a up to 10% of cobalt (where the solubility limit is reached) is due to substitution of Ce^{4+} by Co^{2+} or Co^{3+}. For higher cobalt content, the strain caused by increasing molar fraction of oxygen vacancies is more pronounced than the ionic radius difference between Ce^{4+} and Co^{2+}/Co^{3+}, resulting in an increase in a. Thus, the results suggest that cobalt is well dispersed in the volume and/or on the surface of ceria for both (5)Co/CeO_2 and (10)Co/CeO_2 samples, whilst for (15)Co/CeO_2 and (20)Co/CeO_2, cobalt is most likely residing on the surface of ceria and forming Co_3O_4 precipitates.

Fig. 2 presents the UV–Vis diffuse reflectance spectra for the samples. Pure CeO_2 showed three characteristics peaks, at 226, 305 and 345 nm, assigned as $f \rightarrow d$ transitions of Ce^{3+} species, localized O → Ce charge transfer transition involving a number of surface Ce^{4+} ions and interband transitions in CeO_2, respectively [36,37]. The band around 430–450 is due transitions of octahedral Co^{3+}, and the band centered at 730 nm is due to transitions of octahedral Co^{3+} [38]. The band around 305 nm becomes less intense with increasing cobalt content. It is possible that surface Ce^{4+} ions are

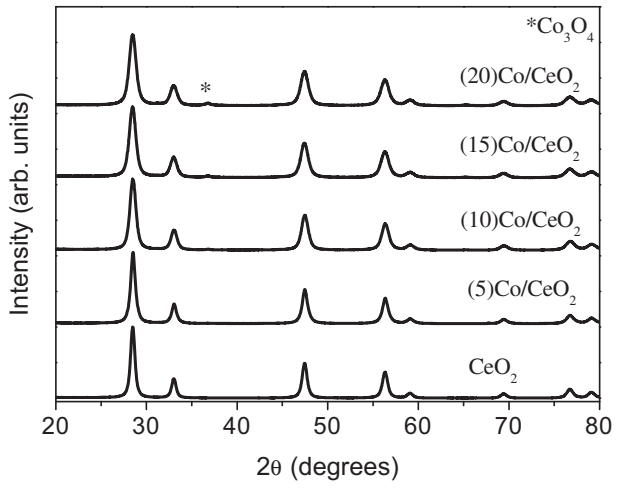

Fig. 1. XRD patterns of ceria-supported cobalt samples.

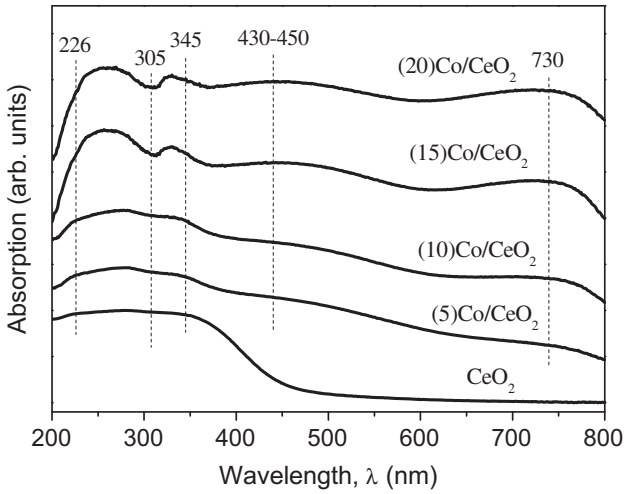

Fig. 2. UV–Vis spectra of the ceria-supported cobalt samples.

substituted by Co^{3+} and/or Co^{2+} ions. This result is consistent with our previous assumption presented with XRD results that cobalt most likely resides on surface sites of the ceria.

Fig. 3 presents SEM-FEG images of the prepared samples. One can see the presence of agglomerates made of nanoparticles with average size between 10 and 20 nm for CeO_2 sample and between 20 and 30 nm for the samples with cobalt. These results are in agreement with our d_{eq} data calculated via BET measurements.

The determination of reducible species at the surface of the catalyst and the temperature at which these species are reduced give important information regarding catalytic performance. The TPR profiles of the ceria-supported cobalt samples used as catalysts in this study are presented in Fig. 4. The aforementioned structural differences imply different reduction patterns that were discussed according to the literature data [39–45]. The TPR spectrum of CeO_2 may contain one to three peaks. A first peak, at around 450 °C, is usually ascribed to the reduction of the ceria surface; a second peak at 580 °C, which is due to the formation of non-stoichiometric oxides of composition CeO_x; and a third peak at 920 °C, which indicates the reduction of CeO_2 to Ce_2O_3 in the bulk sample. Nevertheless, according to Holgado et al. [45] the highest temperature TPR peak could also be indicating that the reduction of CeO_2 goes to CeO_{2-x}. In the case of Co_3O_4, the reduction process is described as a two step process ($Co_3O_4 \rightarrow CoO \rightarrow Co$) with two types of H_2–TPR profiles, one consisting of a broad peak and the other presenting two defined peaks. All TPR profiles of the samples studied in this work have two regions where hydrogen is consumed: a low temperature range (350–700 °C) and a high-temperature range (700–1000 °C). The XRD data indicates that there is no cobalt secondary phase in the (5)Co/CeO_2 sample, while its TPR profile displays two main reduction peaks. The first one, a weak and broad peak with a maximum at around 450 °C and a little shoulder centered at 500 °C corresponding to the reduction of Co_3O_4 phase to CoO and the reduction of CoO to Co^0, respectively. However, we cannot rule out the reduction of surface ceria, which occurs at low temperatures (around 450 °C). Thus, the first broad reduction peak could also comprise the reduction of surface ceria due to the low cobalt content in this sample. The second, a high-temperature peak centered at 900 °C, can be ascribed to the reduction of Ce^{4+} to Ce^{3+} in the bulk of ceria. Furthermore, this characteristic peak (with a maximum at around 900 °C) was observed in the TPR profiles of all samples. A careful observation of the TPR curve for this sample shows the presence of a very weak and broad peak centered at around 680 °C that can be attributed to

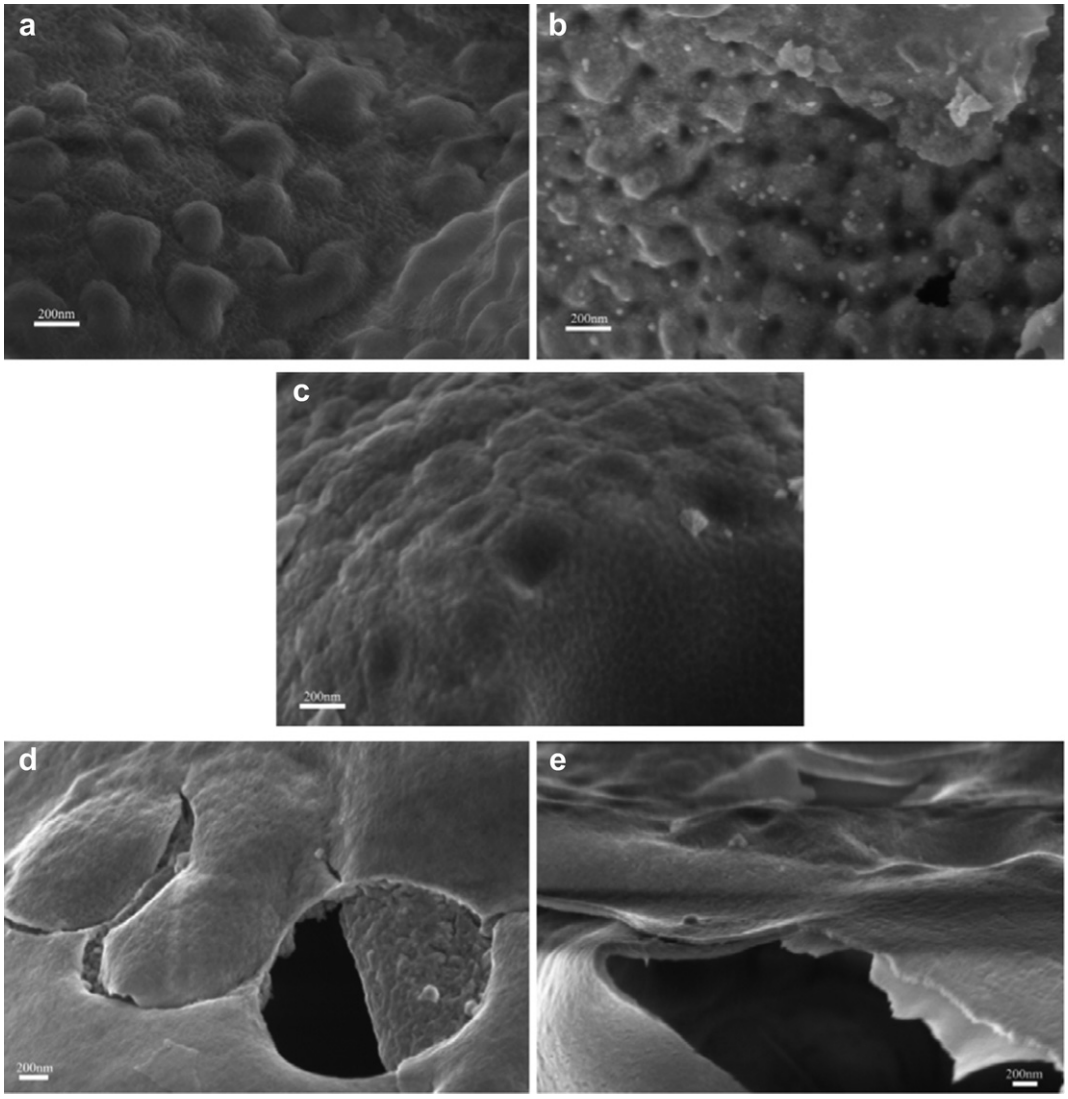

Fig. 3. SEM-FEG images for ceria-supported cobalt samples: (a) CeO_2, (b) (5)Co/CeO_2, (c) (10)Co/CeO_2, (d) (15)Co/CeO_2 and (e) (20)Co/CeO_2.

the reduction of Co^{2+} or Co^{3+} linked to the support. The TPR profile of the (10)Co/CeO_2 sample shows three major H_2 consumption peaks. The lower temperature peak can be rationalized by the reduction of Co_3O_4 phase to CoO while the second peak, centered at 580 °C, results from the reduction of Co^{2+} or Co^{3+} ions strongly bound in the ceria matrix. Nevertheless, this second peak could also comprise the reduction of non-stoichiometric species, as mentioned before. The reduction of CoO to Co^0 can be identified by the shoulder centered at 515 °C present in the second peak. The TPR profile of the (20)Co/CeO_2 sample shows four major H_2 consumption peaks. The lower temperature peak, observed at 390 °C, can be attributed to the reduction of the Co_3O_4 phase to CoO while the second peak, centered at 460 °C, to the subsequent reduction of CoO to Co^0. Finally, the third peak at around 595 °C indicates the reduction of Co^{2+} or Co^{3+} ions in a strong interaction with the CeO_2 and it could also be compromising the reduction of the CeO_x species. Interestingly, a pattern was observed wherein cobalt loading was responsible for the step-wise reduction of cobalt oxide shifting to a lower temperature. This suggests that the reduction process of the samples becomes easier with higher cobalt content. In addition, the broad peak, attributed to the reduction of surface Ce^{4+} to Ce^{3+} ions, present in the TPR profiles decreased in intensity with increasing cobalt content, indicating that cobalt substitutes Ce^{4+} ions located in the surface of ceria as the cobalt content increases. These results are consistent with our previous assumption presented by the XRD and UV–Vis results showing that cobalt is well distributed in the volume and/or on the surface of ceria for (5)Co/CeO_2 and (10)Co/CeO_2 samples and as the cobalt content increases it is more likely to be located and dispersed on the surface of ceria forming Co_3O_4 precipitates when the solubility limit is exceeded.

3.2. Catalytic tests

In order to investigate the catalytic activity of the samples, the steam reforming of ethanol was carried out. The influence of different operating temperatures on the ethanol conversion and product distribution was studied by varying the temperature from 400 to 600 °C. The catalytic behaviors of the different ceria-supported cobalt samples ((5)Co/CeO_2, (10)Co/CeO_2 and (20)Co/CeO_2) were also studied and compared. Typical experimental results obtained are presented in Figs. 5 and 7, in which the selectivity of each product and the conversion of ethanol are shown as a function of reaction time. It was observed that the ethanol

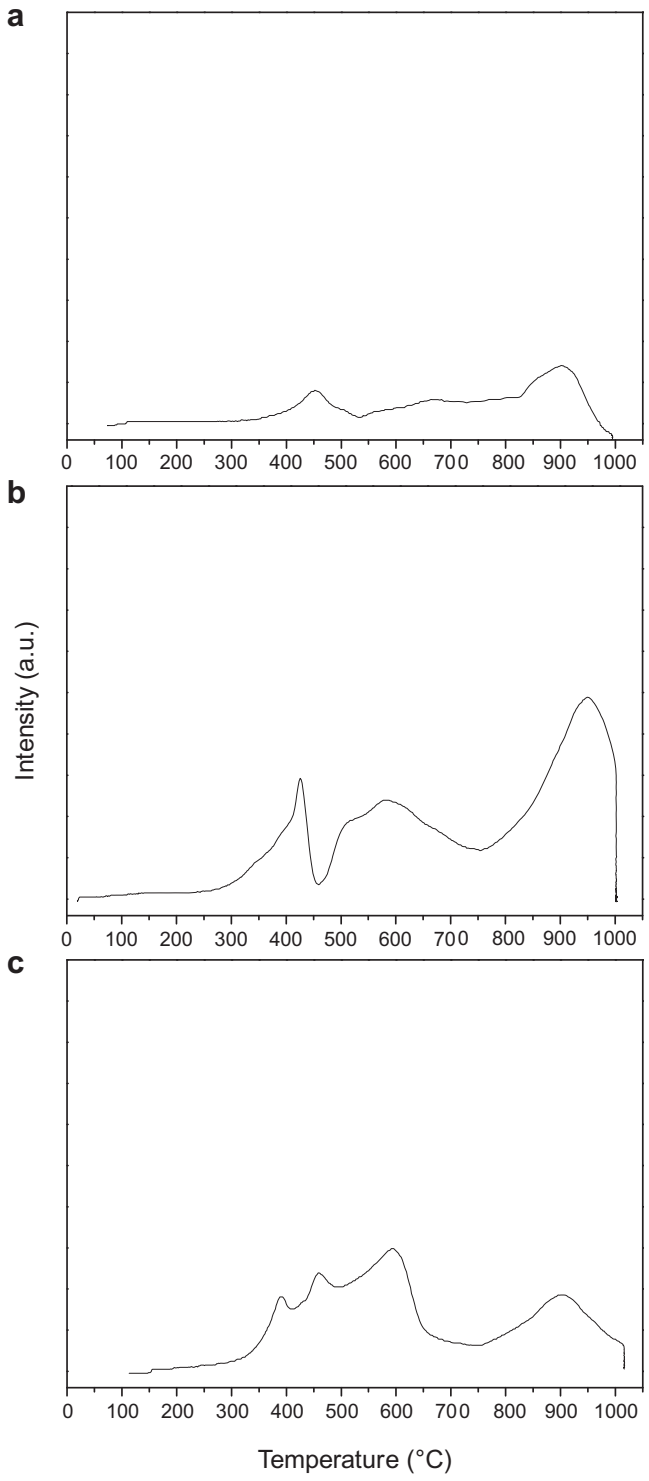

Fig. 4. TPR profiles for ceria-supported cobalt samples: (a) (5)Co/CeO_2, (b) (10)Co/CeO_2 and (c) (20)Co/CeO_2.

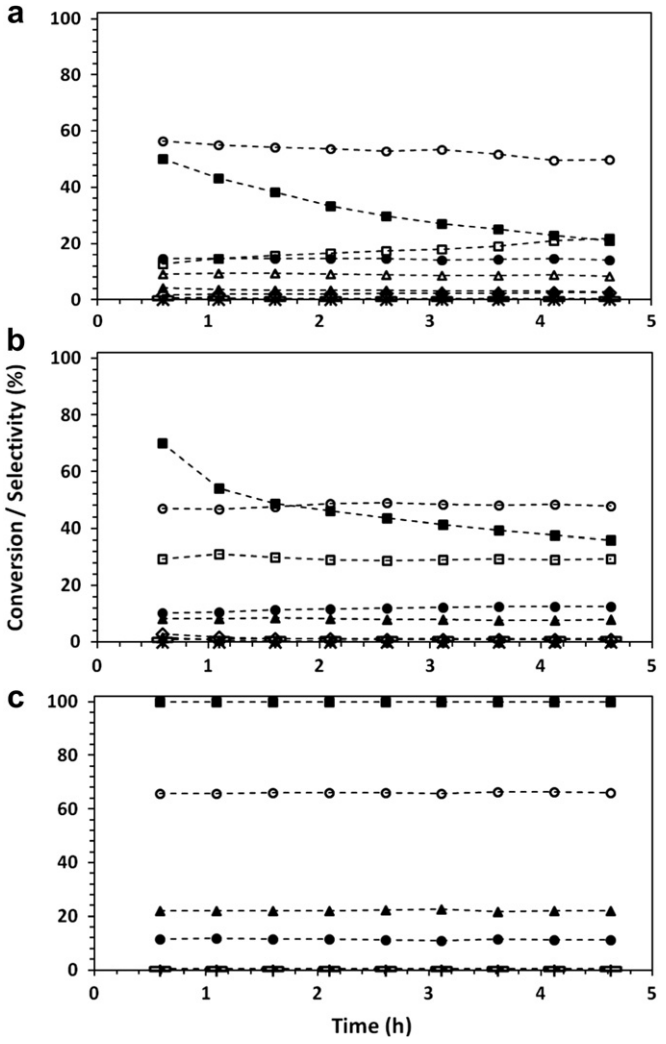

Fig. 5. Steam reforming of ethanol over (20)Co/CeO_2catalyst at different temperatures: (a) 400 °C, (b) 500 °C and (c) 600 °C. Legends: Filled square = C_2H_5OH conversion, open circle = H_2, filled circle = CO_2, open square = CH_3CHO, open triangle = CH_3COCH_3, filled triangle = CO, open rhombus = C_2H_4, open rectangle = CH_4, plus symbol = C_2H_6, multiplication symbol = C_3H_6, selectivities respectively.

steam reforming experiments performed over supported cobalt catalysts showed an ethanol conversion levels and product distribution that varied with reaction temperature and the nature of the catalyst. The effect of reaction temperature on catalytic performance of (20)Co/CeO_2 catalyst in the steam reforming of ethanol was investigated and the results are presented in Fig. 5. As expected, the conversion of ethanol increased with increasing reaction temperature. The complete conversion of ethanol was achieved when the temperature employed was 600 °C. Nine compounds were observed in the reaction effluent during the ethanol steam reforming process in the range of reaction temperatures studied. Six of those, H_2 (hydrogen), CO_2 (carbon dioxide), CO (carbon monoxide), C_2H_4 (ethylene), CH_3CHO (acetaldehyde) and CH_3COCH_3 (acetone) were the major products detected. Another three compounds, CH_4 (methane), C_2H_6 (ethane) and C_3H_6 (propylene) were minor products formed where the selectivity to each one was always less than 2% in all tests. At 400 °C, the conversion of ethanol reached 50% at the beginning of the test. However, the ethanol conversion decreased to 21% after 300 min in time on stream with little difference in product distribution. The process at this temperature had a high selectivity toward hydrogen production and mainly CO_2, CH_3CHO and CH_3COCH_3 were formed as byproducts, with lower amounts of CO and C_2H_4, indicating that the steam reforming of ethanol (reaction 1), ethanol dehydrogenation to acetaldehyde (reaction 2) and aldol condensation reaction of acetaldehyde molecules to form acetone (reaction 3), seem to occur as the main side reactions. Acetone is not a very common

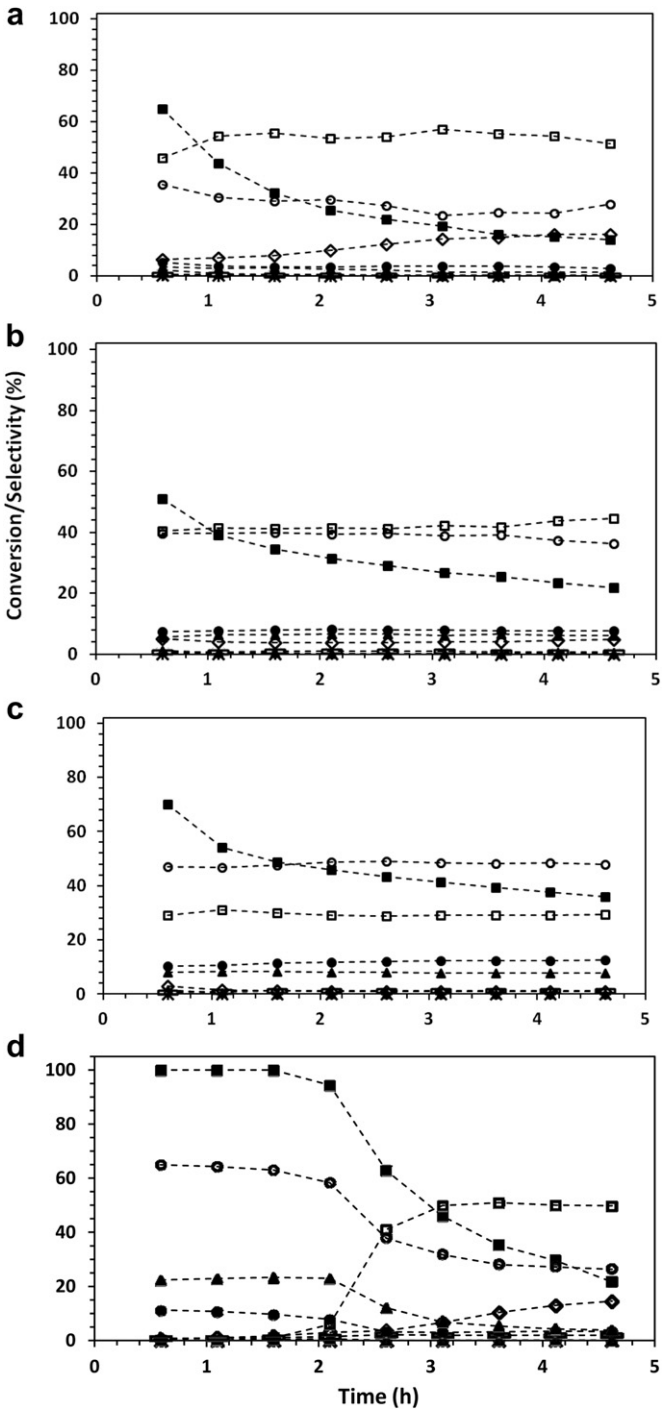

Fig. 6. Steam reforming of ethanol at reaction temperature of 500 °C over: (a) (5)Co/CeO_2, (b) (10)Co/CeO_2, (c) (20)Co/CeO_2 catalysts and (d) At reaction temperature of 600 °C over (5)Co/CeO_2 catalyst. Legends: Filled square = C_2H_5OH conversion, open circle = H_2, filled circle = CO_2, open square = CH_3CHO, open triangle = CH_3COCH_3, filled triangle = CO, open rhombus = C_2H_4, open rectangle = CH_4, plus symbol = C_2H_6, multiplication symbol = C_3H_6, selectivities respectively.

product from the ethanol steam reforming process. However, its production can be related to CeO_2 used as support. According to Wang et al. [19] CeO_2-based catalysts can favor acetaldehyde condensation to acetone. In addition, Nishiguchi et al. [20] have studied the formation mechanism of acetone in steam reforming of ethanol suggesting its production from acetaldehyde. The amount of ethylene detected (close to 2%) could indicate that this particular catalyst has few acid sites which are capable of dehydrating small amounts of ethanol (reaction 4) at this temperature.

$$C_2H_5OH + 3H_2O \rightarrow 2CO_2 + 6H_2 \quad (1)$$

$$C_2H_5OH \rightarrow CH_3CHO + H_2 \quad (2)$$

$$2CH_3CHO \rightarrow CH_3COCH_3 + CO + H_2 \quad (3)$$

$$C_2H_5OH \rightarrow C_2H_4 + H_2O \quad (4)$$

Similarly, a deactivation behavior was observed when the reaction temperature was increased to 500 °C, and this was also accompanied by a decrease in the selectivity for H_2. In contrast, the selectivity of CH_3CHO and CO increased but on the other hand the selectivity to CO_2 slightly decreased and practically no CH_3COCH_3 was detected. This indicates that at this stage the steam reforming of ethanol (reaction (1)), ethanol dehydrogenation (reaction (2)) and reverse water gas shift reaction (reaction (5)) was taking place and thus these reactions are favored at this temperature.

$$CO_2 + H_2 \rightarrow CO + H_2O \quad (5)$$

At the highest evaluated reaction temperature, the (20)Co/CeO_2 catalyst achieved complete conversion of ethanol and remained stable until the end of the experiment. Selectivity toward H_2 was still high and reached a maximum (close to 66%) at 600 °C. An 8–21% increase in selectivity for CO was observed, whilst the selectivity of CO_2 was almost the same and no acetaldehyde was detected. This indicates that at this stage acetaldehyde decomposed to form CO and CH_4 (reaction (6)) and then, in the presence of water, CH_4 was converted to CO and H_2 by steam reforming (reaction (7)).

$$CH_3CHO \rightarrow CH_4 + CO \quad (6)$$

$$CH_4 + H_2O \rightarrow CO + 3H_2 \quad (7)$$

When the reaction temperature employed was 400 °C and 500 °C, it was observed that ethanol conversions decreased with time on stream. On the other hand, when the reaction temperature was 600 °C, no catalytic deactivation process was observed. It is well established that deactivation of supported metal catalysts during ethanol steam reforming occurs mainly due to carbon deposition on catalyst surface. The nature of carbon deposition with the reaction conditions plays a crucial role in determining the extent of catalyst deactivation. Commonly, two types of carbonaceous deposits, which depend on the operational conditions, have been reported, amorphous carbon and filamentous carbon. The first type leads to severe deactivation while the second leads to a mild deactivation process [40]. In this work, the quantitative determination of coke deposited, as well as the type of carbon formed and its influence on the catalytic behavior is not reported. This study is under way and it will be reported in due course. However, it is known that the reaction pathway during catalytic ethanol steam reforming comprises a series of simultaneous reactions, including decomposition, dehydrogenation, dehydration and steam reforming reactions. These reactions are more or less promoted depending on the nature of the catalyst, the type of interaction with the surface of the solid material and the different reaction conditions [11–14]. In our case, from the catalytic results in the reaction temperature range of 400–500 °C, the detected reaction products were especially comprised of H_2, CO_2, CH_3CHO and CH_3COCH_3. Thus, we can speculate that coke mainly comes from CH_3CHO and CH_3COCH_3. Ethanol is dehydrogenated to produce acetaldehyde and hydrogen (reaction (2)) and then the acetaldehyde is converted to acetone

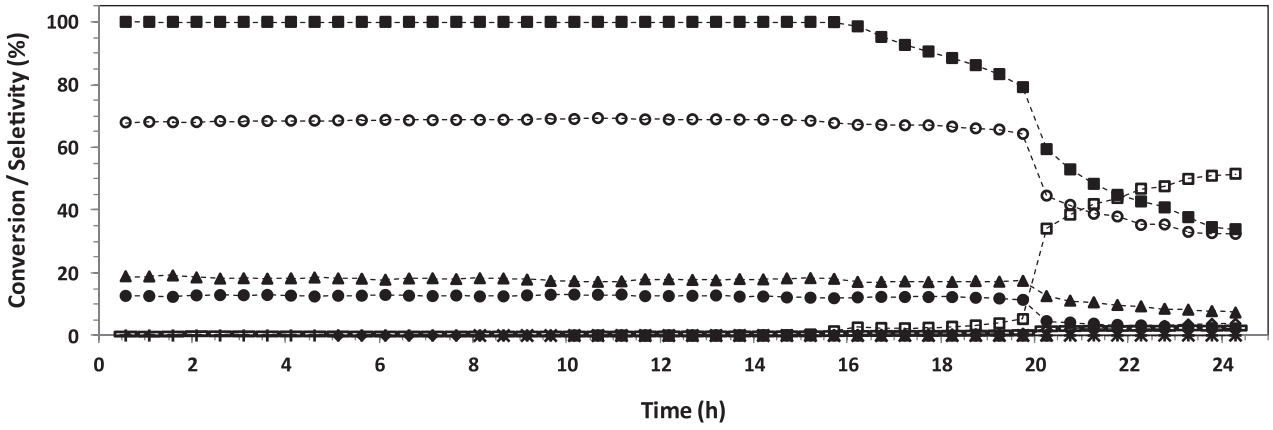

Fig. 7. Long-term stability test of (20)Co/CeO_2 catalyst at reaction temperature of 600 °C. Legends: Filled square = C_2H_5OH conversion, open circle = H_2, filled circle = CO_2, open square = CH_3CHO, open triangle = CH_3COCH_3, filled triangle = CO, open rhombus = C_2H_4, open rectangle = CH_4, plus symbol = C_2H_6, multiplication symbol = C_3H_6, selectivities respectively.

(reaction (3)), these products can be precursors of coke formation from reactions (8) and (9), leading to catalyst deactivation. It is important to note that the decomposition of methane reaction to hydrogen and carbon (reaction (10)) cannot be ruled out due to the low concentrations of the hydrocarbon detected, which can also contribute partly to carbon deposition. When the reaction temperature was 600 °C, H_2, CO_2 and CO were the main compounds detected while CH_3CHO and CH_3COCH_3 were not detected and no catalyst deactivation was observed. This indicate that, even carbon deposition was occurring, this deposition did not affect the activity of the (20)Co/CeO_2 catalyst during the reaction period. Similar behavior for Co/CeO_2 catalysts on ethanol steam reforming was verified by Wang et al. [22], where the process of coke formation or carbon deposition over the catalyst surface was dependent on reaction temperature. According to the authors, when the reaction temperature was 450 °C and lower, ethanol was dehydrogenated and/or dehydrated over Co/CeO_2 catalysts and the dehydrogenated and dehydrated products were further transformed to cokes. On the other hand, when the reaction temperature was 600 °C or higher, carbon deposition was not the main problem for steam reforming of ethanol over Co/CeO_2 catalysts, the coke formation or carbon deposition was hardly seen, neither layered coke nor fiber- or tube-like carbons could be observed.

$$CH_3CHO \rightarrow \text{coke} \quad (8)$$

$$CH_3COCH_3 \rightarrow \text{coke} \quad (9)$$

$$CH_4 \rightarrow 2H_2 + C \quad (10)$$

The effect of cobalt content on catalyst performance was also investigated at different temperatures. Fig. 6 shows ethanol conversion and product selectivities, at 500 and 600 °C, with cobalt content ranging from 5 to 20%. In spite of its lowest specific surface area, the (20)Co/CeO_2 catalyst was the most active among the catalysts tested at 500 °C. The selectivity toward hydrogen increased and the formation of liquid products (acetaldehyde and acetone) decreased with increasing cobalt composition of the catalysts, pointing to the positive effect of cobalt sites for reforming of ethanol molecules. With the increase of metal loading, more cobalt ions were incorporated into CeO_2 lattice, thus a higher number of active sites are available for the reforming reactions that resulted in higher ethanol conversion [19]. On the other hand, ethanol conversions were lower over (5)Co/CeO_2 and (10)Co/CeO_2 catalysts. It is interesting to observe the reaction effluent composition of the (5)Co/CeO_2 catalyst. This particular catalyst was unique in that C_2H_4 appeared in an appreciable extent in the product stream. The physicochemical properties of the catalyst play an important role in the evolution of surface reactions. In ethanol steam reforming both dehydrogenation to acetaldehyde or dehydration to ethylene can occur depending upon the nature of the catalyst. Dehydration and dehydrogenation reactions were promoted over the (5)Co/CeO_2 catalyst surface, thus a combination of catalytic properties could be observed on its surface, this particular catalyst has a great ability for dehydrogenation and a good capability for dehydration of ethanol. This fact can be ascribed to a lower metallic covering on the surface of the support, as determined by XRD, UV–Vis and TPR measurements, indicating that the CeO_2 support is mainly responsible for the catalytic activity in this case. Ethylene and acetaldehyde formation from ethanol steam reforming process over pure CeO_2 operating in a wide range of reaction temperature and inlet C_2H_5OH/H_2O molar ratios have been reported by Laosiripojana et al. [23,24]. With the increase of cobalt content, ethylene production drastically decreases, and it was not detected in the product stream of (20)Co/CeO_2 catalyst. Besides, it can be observed from the results that the selectivity toward CH_3CHO decreased while the production of H_2, CO_2 and CO increased over (20)Co/CeO_2 catalyst, suggesting the promotion of acetaldehyde steam reforming (reaction (11)) and therefore explicates the three reaction steps involving acetaldehyde decomposition (reaction (12)), the water gas shift reaction (reaction (13)), followed by methane steam reforming [46]. This fact may be related to the more effective action of the metal active phase, which is covering a greater surface area of the support due to the greater metal content in this sample. In the presence of cobalt, the catalyst becomes more active for the breaking of the C–C and C–H bonds in the ethanol cleavage to produce hydrogen and C1 compounds, which leads to an improvement in the reforming activity of the catalysts [47–50]. Also, according to the results previously reported [19,25–28], the replacement of some Ce^{4+} with smaller cobalt ions enhances the oxygen storage of CeO_2. This oxygen availability plays an important role in determining both hydrogen yield and the catalyst stability. If there is sufficient oxygen available or accessible, ethanol molecules can be fully oxidized, hindering the formation of byproducts, that results in maximization of hydrogen production, since ethanol steam reforming is considered a redox reaction, where ethanol is oxidized by the oxygen species originating from water present in reaction sphere. This observation is in agreement with the XRD and UV–Vis measurements. In the initial period of the experiments, both (5)Co/CeO_2 and (20)Co/CeO_2 catalysts at

600 °C displayed similar ethanol conversion and product distribution. Ethanol was completely converted and the formation of undesirable reaction byproducts (acetaldehyde and ethylene) was significantly suppressed, during the first 150 min and thus indicates an effective action of the metallic cobalt sites for reforming the ethanol molecules at this temperature. However, it is interesting to note that the ethanol conversion decreased from 100 to 22% after 300 min on stream with a significant difference in the product distribution also being observed. The selectivity toward CH_3CHO appreciably increases and also C_2H_4 increases, with concomitant H_2, CO and CO_2 production decreasing as the reaction progresses over time, indicating that at this stage ethanol dehydrogenation becomes the main reaction involved. This fact can be related to the coke formation from ethylene polymerization (reaction (14)) and acetaldehyde (reaction (8)). As mentioned before, the amount of active phase available from this catalyst is lower and so when the active metal phase is covered due to encapsulation by carbon, the active sites would be less accessible and the support would be mainly responsible for the catalytic activity in this case, leading to CH_3CHO and C_2H_4 formation [51]. In addition, this may be considered as the main reason for the catalyst deactivation that was observed, in spite of this, loss of activity for the cobalt-based catalysts can also be related to the oxidation of metallic Co particles during the reaction [52].

In order to investigate the (20)Co/CeO_2 catalyst stability, a long-term reaction test was performed at 600 °C (Fig. 7). Ethanol conversion achieved 100% and was totally stable for approximately 17 h. The selectivity to hydrogen was high and remained constant during 20 h on time on stream. After 20 h of reaction, a similar catalytic behavior to that of (5)Co/CeO_2 in the final part of the experiment at 600 °C was observed with an increase in acetaldehyde formation, a decrease in the H_2, CO and CO_2 selectivities and catalyst deactivation which is most probably due to carbon deposition on its surface.

$$CH_3CHO + H_2O \rightarrow CO_2 + CH_4 + H_2 \quad (11)$$

$$CH_3CHO \rightarrow CO + CH_4 \quad (12)$$

$$CO + H_2O \rightarrow CO_2 + H_2 \quad (13)$$

$$C_2H_4 \rightarrow \text{coke} \quad (14)$$

4. Conclusions

In this study, ceria-supported cobalt catalysts were prepared trough the polymeric precursor method. The preparative methodology employed led to the obtainment of materials with important properties for applications in catalytic processes, such as ethanol steam reforming for hydrogen production. Structural and optical characterization revealed that cobalt is well distributed in the volume and/or on the surface of ceria for (5)Co/CeO_2 and (10)Co/CeO_2 samples and as the cobalt content increases it is more likely to be located and dispersed on the surface of ceria forming Co_3O_4 precipitates when the solubility limit is exceeded. According to XRD, UV–Vis and TPR measurements, cobalt content in the catalyst influences the metal-support interaction which results in distinct catalyst performances. The results clarify that the reaction conditions and the nature of the catalysts influenced the ethanol steam reforming process. The (20)Co/CeO_2 catalyst showed the best performance among the catalysts tested, exhibiting a high ethanol conversion and hydrogen selectivity, at 600 °C of reaction temperature, where ethanol was completely consumed and the selectivity to hydrogen reached approximately 66%. A long-term test conducted at 600 °C showed that the (20)Co/CeO_2 catalyst is acceptably stable and could be considered as a good candidate for hydrogen production from ethanol steam reforming.

Acknowledgments

This research was supported by the Brazilian funding support agencies: FAPESP, CAPES, CNPq and FAPEMIG. The authors are indebted to Prof. Elson Longo and Prof. Rorivaldo de Camargo for the FE-SEM images. Authors would also like to thank Prof. Jason G. Taylor for insightful discussion and for reviewing the manuscript for its English usage.

References

[1] R. Kothari, D. Buddhi, R.L. Sawhney, Renew. Sustain Energy Rev. 12 (2008) 553–563.
[2] F. Joensen, J.R. Rostrup-Nielsen, J. Power Sources 105 (2002) 195–201.
[3] J.N. Armor, Catal. Lett. 101 (2005) 131–135.
[4] T. Abbasi, S.A. Abbasi, Renew. Sustain Energy Rev. 15 (2011) 3034–3040.
[5] F. de Bruijn, Green Chem. 7 (2005) 132–150.
[6] J.L. Silveira, L.B. Braga, A.C.C. de Souza, J.S. Antunes, R. Zanzi, Renew. Sustain Energy Rev. 13 (2009) 2525–2534.
[7] H. Song, U.S. Ozkan, Int. J. Hydrogen Energy 35 (2010) 127–134.
[8] P. Ramírez de la Piscina, N. Homs, Chem. Soc. Rev. 37 (2008) 2459–2467.
[9] F. Díaz Alvarado, F. Gracia, Chem. Eng. J. 165 (2010) 649–657.
[10] V. Mas, R. Kipreos, N. Amadeo, M. Laborde, Int. J. Hydrogen Energy 31 (2006) 21–28.
[11] A. Haryanto, S. Fernando, N. Murali, S. Adhikari, Energy Fuels 19 (2005) 2098–2106.
[12] P.D. Vaidya, A.E. Rodrigues, Chem. Eng. J. 117 (2006) 39–49.
[13] M. Ni, D.Y.C. Leung, M.K.H. Leung, Int. J. Hydrogen Energy 32 (2007) 3238–3247.
[14] A. Bshish, Z. Yaakob, B. Narayanan, R. Ramakrishnan, A. Ebshish, Chem. Pap. 65 (2011) 251–266.
[15] H. Song, B. Tan, U.S. Ozkan, Catal. Lett. 132 (2009) 422–429.
[16] J.Y. Siang, C.C. Lee, C.H. Wang, W.T. Wang, C.Y. Deng, C.T. Yeh, et al., Int. J. Hydrogen Energy 35 (2010) 3456–3462.
[17] F. Wang, W. Cai, H. Provendier, Y. Schuurman, C. Descorme, C. Mirodatos, et al., Int. J. Hydrogen Energy 36 (2011) 13566–13574.
[18] J.L. Ye, Y.Q. Wang, Y. Liu, H. Wang, Int. J. Hydrogen Energy 33 (2008) 6602–6611.
[19] H. Wang, J.L. Ye, Y. Liu, Y.D. Li, Y.N. Qin, Catal. Today 129 (2007) 305–312.
[20] T. Nishiguchi, T. Matsumoto, H. Kanai, K. Utani, Y. Matsumura, W.J. Shen, et al., Appl. Catal. A 279 (2005) 273–277.
[21] H.V. Fajardo, L.F.D. Probst, N.L.V. Carreño, I.T.S. Garcia, A. Valentini, Catal. Lett. 119 (2007) 228–236.
[22] H. Wang, Y. Liu, L. Wang, Y.N. Qin, Chem. Eng. J. 145 (2008) 25–31.
[23] N. Laosiripojana, S. Assabumrungrat, Appl. Catal. B 66 (2006) 29–39.
[24] N. Laosiripojana, W. Sutthisripok, S. Assabumrungrat, Chem. Eng. J. 127 (2007) 31–38.
[25] L.F. Liotta, G. Di Carlo, G. Pantaleo, G. Deganello, Catal. Commun. 6 (2005) 329–336.
[26] H. Song, U.S. Ozkan, J. Catal. 261 (2009) 66–74.
[27] H. Song, L. Zhang, U.S. Ozkan, Ind. Eng. Chem. Res. 49 (2010) 8984–8989.
[28] B. Bayram, I.I. Soykal, D. von Deak, J.T. Miller, U.S. Ozkan, J. Catal. 284 (2011) 77–89.
[29] A.A. Rabelo, M.C. de Macedo, D.M.A. Melo, C.A. Paskocimas, A.E. Martinelli, R.M. do Nascimento, Mater. Res. 14 (2011) 91–96.
[30] V.D. Araújo, M.I.B. Bernardi, J. Therm. Anal. Calorim. 103 (2011) 501–506.
[31] A.C. Larson, R.B.V. Dreele. In Los Alamos Natl. Lab. Rep. LAUR 86-748, 1994.
[32] X. Wang, J.A. Rodriguez, J.C. Hanson, D. Gamarra, A. Martínez-Arias, M. Fernández-García, J. Phys. Chem. B 110 (2006) 428–434.
[33] S. Kumar, Y.J. Kim, B.H. Koo, H. Choi, C.G. Lee, Trans. Magnetics 45 (2009) 2439–2441.
[34] R. Shannon, Acta Crystallogr. A 32 (1976) 751–767.
[35] J.E. Spanier, R.D. Robinson, F. Zhang, S.W. Chan, I.P. Herman, Phys. Rev. B 64 (2001) 245407–245414.
[36] A. Bensalem, J.C. Muller, F. Bozon-Verduraz, J. Chem. Soc. Faraday Trans. 88 (1992) 153–154.
[37] C.W. Tang, C.C. Kuo, M.C. Kuo, C.B. Wang, S.H. Chien, Appl. Catal. A 309 (2006) 37–43.
[38] Y. Brik, M. Kacimi, M. Ziyad, F. Bozon-Verduraz, J. Catal. 202 (2001) 118–128.
[39] A.A. Firsova, T.I. Khomenko, A.N. Il'ichev, V.N. Korchak, Kinet. Catal. 49 (2008) 682–691.
[40] S.M. de Lima, A.M. da Silva, L.O.O. da Costa, U.M. Graham, G. Jacobs, B.H. Davis, et al., J. Catal. 268 (2009) 268–281.
[41] M. Kang, M.W. Song, C.H. Lee, Appl. Catal. A 251 (2003) 143–156.

[42] L. Spadaro, F. Arena, M.L. Granados, M. Ojeda, J.L.G. Fierro, F. Frusteri, J. Catal. 234 (2005) 451–462.
[43] F. Wyrwalski, J.M. Giraudon, J.F. Lamonier, Catal. Lett. 137 (2010) 141–149.
[44] C.B. Wang, C.C. Lee, J.L. Bi, J.Y. Siang, J.Y. Liu, C.T. Yeh, Catal. Today 146 (2009) 76–81.
[45] J.P. Holgado, R. Alvarez, G. Munera, Appl. Surf. Sci. 161 (2000) 301–315.
[46] A.F. Lucrédio, J.A. Bellido, E.M. Assaf, Catal. Commun. 12 (2011) 1286–1290.
[47] D.R. Sahoo, S. Vajpai, S. Patel, K.K. Pant, Chem. Eng. J. 125 (2007) 139–147.
[48] S.S.Y. Lin, D.H. Kim, S.Y. Ha, Appl. Catal. A 355 (2009) 69–77.
[49] M.S. Batista, R.K.S. Santos, E.M. Assaf, J.M. Assaf, E.A. Ticianelli, J. Power Sources 124 (2003) 99–103.
[50] J. Llorca, N. Homs, J. Sales, J.L.G. Fierro, P. Ramírez de la Piscina, J. Catal. 222 (2004) 470–480.
[51] P. Ciambelli, V. Palma, A. Ruggiero, Appl. Catal. B 96 (2010) 18–27.
[52] E.B. Pereira, N. Homs, S. Martí, J.L.G. Fierro, P. Ramírez de la Piscina, J. Catal. 257 (2008) 206–214.